Geometric compatibility assessment of the integrated edge-ramp model based on architectural traces in the pyramid of Khafre

Vicente Luis Rosell Roig.

vicente.rosell@gmail.com

L'Alcúdia. 46250. Valencia. Spain.

Supplementary Material

Contents

Note: References correspond to the numbering used in the main manuscript.

S1. Comparison between Khafre and Khufu

Table S1.1. Geometry and global magnitudes

Parameter	Khufu (G1)	Khafre (G2)	Comparison / implication IER
Original height	146.6 m	143.5 m	G2 is 3.1 m lower (≈ 0.9789×)
Current height	138.5 m	136.4 m	G2 appears "taller" due to the terrain elevation (it is not geometric height)
Base side	230.3 m	215.25 m	G2 is 15.05 m smaller (≈ 0.9347×)
Volume	2.6×10^6 m³	2.2×10^6 m³	G2 ≈ 0.8504× the volume of G1
Face angle (slope)	51°50′40″	53.13°	G2 is steeper, which affects the predicted IER turning and band elevations.

Table S1.2. Surface, limestone, casing and visible "bands"

Issue	Khufu (G1)	Khafre (G2)	IER implication / observables
Casing	Almost everything is lost; only isolated remnants remain (base/areas)	The only one of the three large ones that retains casing on the top	G2 provides a useful comparative case for assessing how preserved casing and casing-loss bands affect elevation-based interpretation.
"Lower limit" of the preserved casing	—	Visible as a macroscopic transition in the upper third (casing →core)	Approximate upper-third transition, broadly around 100–120 m depending on face and preservation state; this value is treated as a macroscopic altimetric marker rather than a direct measurement
Surface bands / discontinuities	In G1 there are facade phenomena (e.g., concavity/indentations discussed in the literature)	more regular masonry band is very visible in the middle (described in general sources)	In IER, the bands may correspond to reconfigurations of ramps / turns / channel closures
Materials (high level)	Local limestone + Tura limestone for casing + granite (king's chamber)	Limestone (blocks >2 t) and temple complexes with megaliths; maintains casing above	For IER: slope difference dominates geometric band prediction; lithology affects friction/erosion

Table S1.3. Logistic scale: blocks, masses, times.

Issue	Khufu (G1)	Khafre (G2)
Number of blocks (estimate)	$\approx2.3\times10^6$	$\approx2.0\times10^6$ (≈ 0.8696 ×)
Average height of the block	0.71 m	0.70 m
Block width (square)	1.27 m	1.27 m
Block mass (average)	2,267.96 kg	2,267.96 kg
Construction duration (typical estimate)	~27 years	~25 years
Direct logistical evidence	Merer's Diary (deliveries of Tura limestone in year 27 of Khufu) appears in general summaries [29]	Based on the analysis of dated texts from the Old Kingdom and the logic of administrative counts [28]

S2. Predicted heights of the IER turns for Khafre

Heights are calculated from the original base of the Pyramid of Khafre (B=215.25 m), a face angle β=53.13°, and a constant course height of 0.70 m. For each turn, the continuous height derived from the geometric model is adjusted to the next highest integer multiple of courses, following the operational criteria of the IER algorithm. Dimensions should be interpreted as compatible height ranges, not as direct architectural measurements. In this Supplementary Material, turn denotes a completed perimeter rotation of the edge-integrated corridor; heights are reported as discrete course-aligned cumulative elevations.

Table S2.1. Table S2.1. Cumulative heights of IER-predicted ramp turns for the Pyramid of Khafre. Cumulative heights (in meters) at which the model predicts successive turns of a ramp integrated into the edge, calculated using the discrete IER algorithm, for different ramp angles θ_r.

Turn	**6°**	**6.25°**	**6.5°**	**6.75°**	**7°**	**7.25°**	**7.5°**	**7.75°**	**8°**
0	0	0	0	0	0	0	0	0	0
1	21	21.7	22.4	23.1	24.5	25.2	25.9	26.6	27.3
2	39.2	39.9	41.3	42.7	44.8	45.5	46.9	48.3	49.7
3	54.6	55.3	57.4	58.8	61.6	62.3	64.4	65.8	67.9
4	67.9	68.6	70.7	72.8	75.6	76.3	78.4	80.5	82.6
5	79.1	79.8	81.9	84	87.5	88.2	90.3	92.4	94.5
6	88.9	89.6	91.7	93.8	97.3	98	100.1	102.2	104.3
7	97.3	98	100.1	101.5	105	105.7	107.8	109.9	112
8	104.3	105	107.1	108.5	111.3	112	114.1	116.2	118.3
9	109.9	110.6	112.7	114.1	116.9	117.6	119.7	121.1	123.2
10	114.8	115.5	117.6	119	121.8	121.8	123.9	125.3	127.4
11	119	119.7	121.8	123.2	125.3	125.3	127.4	128.8	130.9
12	122.5	123.2	125.3	126.7	128.8	128.1	130.2	131.6	133.7
13	125.3	126	128.1	129.5	131.6	130.9	132.3	133.7	135.8
14	128.1	128.8	130.2	131.6	133.7	133	134.4	135.8	137.2
15	130.2	130.9	132.3	133.7	135.8	134.4	135.8	137.2	138.6
16	132.3	133	133.7	135.1	137.2	135.8	137.2	138.6	140
17	133.7	134.4	135.1	136.5	138.6	137.2	138.6	139.3	140.7
18	135.1	135.8	136.5	137.9	139.3	137.9	139.3	140	141.4
19	136.5	137.2	137.2	138.6	140	138.6	140	140.7	142.1
20	137.2	137.9	137.9	139.3	140.7	139.3	140.7	141.4	142.8
21	137.9	138.6	138.6	140	141.4	140	141.4	142.1	
22	138.6	139.3	139.3	140.7	142.1	140.7			
23	139.3	140	140	141.4					

S3. Comparison of IER turns with course thickness changes

To assess sensitivity to reading uncertainty and course-by-course discretization, each detected course-height change was first expanded to a raw tolerance window of ±1.40 m (two nominal courses for hb = 0.70 m). These raw windows are reported in Table S3.1 to document the source detections used in the comparison. Because several adjacent windows overlap, they were subsequently merged into consolidated, non-overlapping elevation bands (B*) for interpretive comparison with IER-predicted turn heights; these consolidated bands are reported in Table S3.2.

In addition to the course-height change bands used in the main comparison, R16 is reported as an observational range associated with the NW corner notch, estimated at approximately 100 m. Its inclusion is documentary: it records whether any independently predicted IER turn falls within the same predeclared tolerance window. R16 is not used to recalibrate θ_r, to modify the matching criteria, or to optimize the selected ramp angle.

Table S3.1. Correspondence between raw course-change windows (±1.40 m) and IER-predicted turn heights for different ramp angles. Each row defines a vertical range associated with significant variations in course thickness observed in the Pyramid of Khafre (G2). The cells indicate the IER turn height that falls within each range, when there is a match. Additionally, R16 reports the observational range associated with the flat NW corner notch (~100 m). This range includes IER-predicted heights for more than one slope/turn combination; the $\theta_r \approx 7.5°$ case is discussed in the main text because it places Turn 6 within this range, preserving the selected reference turn-order relationship. R16 is therefore treated as an observational marker, not as a recalibration criterion. The last row reports, as a descriptive indicator only, the number of raw windows containing at least one IER turn for each angle. Because some R* windows overlap, this count is not used as the independent interpretive match count; the conservative comparison is provided in Table S3.2.

Range	Elevation (m)	6°	6.25°	6.5°	6.75°	7°	7.25°	7.5°	7.75°	8°
R1	6.10–8.90									
R2	13.95–16.75									
R3	16.12–20.07									
R4	25.85–28.65							25.9	26.6	27.3
R5	28.23–31.03									
R6	31.77–34.57									
R7	35.23–38.03									
R8	37.79–40.59	39.2	39.9							
R9	40.51–43.31			41.3	42.7					
R10	42.56–45.36				42.7	44.8				
R11	45.79–48.59							46.9	48.3	
R12	60.14–64.38						61.6	64.4		
R13	66.87–69.67	67.9	68.6							67.9
R14	69.78–74.12			70.7	72.8					
R15	79.52–82.32		79.8	81.9					80.5	
R16	98.6-101.4			100.1				100.1		
R17	108.40–111.20	109.9	110.6		108.5				109.9	
Total	Raw window matches	3	4	4	4	1	1	4	4	2

To avoid treating closely spaced course-height changes as independent observations, the original raw ranges (R*) were converted into consolidated elevation bands (B*). Each raw range was first defined by expanding a detected course-height change by ±1.40 m, corresponding to approximately two nominal courses. When two or more resulting windows overlapped, they were merged into a single non-overlapping band representing one broader altimetric adjustment zone rather than multiple separate events. This consolidation reduces the risk of double-counting a single IER-predicted turn within the same local construction transition and provides a more conservative basis for comparing model-predicted turn heights with observable course-height patterns. The original R* intervals are therefore treated as source detections, whereas the consolidated B* bands are used for interpretive comparison. The NW corner notch is reported separately because it is a localized point feature, not a course-height band.

Table S3.2. Consolidated non-overlapping elevation bands (B*) derived from course-height change windows in the Pyramid of Khafre (G2), compared with IER-predicted turn heights for ramp angles between 6° and 8°. Raw R* windows were merged when overlapping, so that each B* band represents one independent altimetric adjustment zone. Table S3.2, rather than the raw R* count in Table S3.1, provides the conservative interpretive basis for evaluating relative correspondence patterns across ramp angles. The NW corner notch is reported separately as N1 because it is a localized point feature, not a course-height band. Counts are therefore given separately for course-height bands only and for the same comparison including N1. Note: the 64.4 m value is retained because IER turn heights are reported to one decimal place; with one-decimal rounding, it falls within the effective upper boundary of B7.

Band	**Source range(s)**	**Elevation band (m)**	**6°**	**6.25°**	**6.5°**	**6.75°**	**7°**	**7.25°**	**7.5°**	**7.75°**	**8°**
B1	R1	6.10–8.90									
B2	R2–R3	13.95–20.07									
B3	R4–R5	25.85–31.03							25.9	26.6	27.3
B4	R6	31.77–34.57									
B5	R7–R10	35.23–45.36	39.2	39.9	41.3	42.7	44.8				
B6	R11	45.79–48.59							46.9	48.3	
B7	R12	60.14–64.38					61.6	62.3	64.4		
B8	R13	66.87–69.67	67.9	68.6							67.9
B9	R14	69.78–74.12			70.7	72.8					
B10	R15	79.52–82.32		79.8	81.9					80.5	
N1	R16	98.60–101.40			100.1				100.1		
B11	R17	108.40–111.20	109.9	110.6		108.5				109.9	
Total, B bands only			3	4	3	3	2	1	3	4	2
Total, including N1			3	4	4	3	2	1	4	4	2

Because IER-predicted turn elevations become progressively closer together as the pyramid narrows toward the apex, correspondences at higher elevations have lower discriminatory power than those in the lower and middle parts of the monument. In other words, the probability of a predicted turn falling near an observed elevation band increases with height simply because the vertical spacing between successive turns decreases. For this reason, lower- and mid-level matches are treated as more informative constraints, whereas upper-level correspondences are interpreted more cautiously as compatibility indicators rather than strong discriminating evidence. Although several ramp angles yield comparable raw match counts, these matches do not carry equal interpretive weight. Under this qualitative weighting, $\theta_r \approx 7.5°$ is retained as the most relevant reference realization because it preserves continuity with the published G1 reference configuration in terms of ramp gradient and traction assumptions, matches lower- to mid-level consolidated bands, and places the homologous Turn 6 within the independently defined NW notch range. The $\theta_r \approx 7.75°$ solution is also retained as a relevant compatible scenario, but with lower interpretive weight because it does not reproduce the homologous Turn 6/NW-notch relationship and because part of its correspondence pattern lies in higher bands with lower discriminatory power. It is therefore treated as a secondary compatible realization rather than as the primary reference case. These selections are not treated as statistical optimizations, but as conservative reference cases combining physical plausibility, turn-order consistency, and the relative discriminatory value of the matched bands. The weighting remains qualitative and does not modify the predefined matching criterion; it only affects the interpretive strength assigned to each correspondence.

Figure S3.1 provides the graphical comparison between the $\theta_r = 7.75°$ predicted turn elevations and the reconstructed course-height profile.

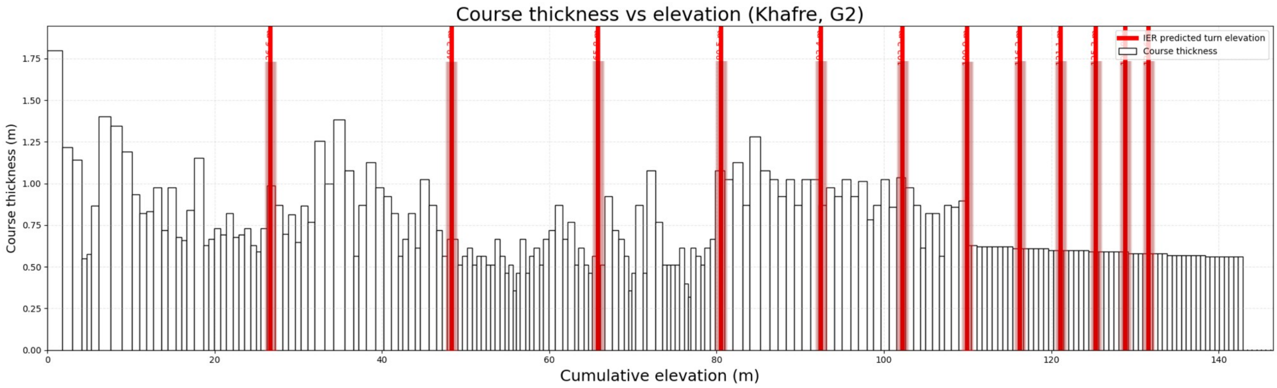

Fig. S3.1. Simulated course height versus cumulative elevation in the Pyramid of Khafre (G2) for a ramp angle $\theta_r = 7.75°$. The white-filled bars with black borders represent the height of each course (m) according to the stratigraphic model reconstructed in this work. The red vertical lines indicate the turn heights predicted by the Integrated Edge-Ramp (IER) model, labelled by their corresponding cumulative elevations (m): 26.6, 48.3, 80.5, and 109.9. Several candidate correspondences are observed between selected predicted turn heights and local increases or decreases in course height, particularly in the middle band of the pyramid and in levels immediately below the preserved casing line. This geometric alignment, derived from independent parameters, does not constitute conclusive proof, but identifies elevation ranges where the operational geometry of the IER can be compared with architectural traces observed in G2, and is presented here as a basis for a more detailed structural and archaeological evaluation.

S4. Additional modeling considerations

While the baseline IER configuration assumes fixed lane geometry, constant crew organization, and homogeneous blocks, real construction likely involved adaptive adjustments as the structure evolved. Variations in block size with height, increasing spatial constraints, and reduced logistical demand would have enabled changes in lane width, crew arrangement, and transport strategies without modifying the underlying geometric framework.

To account for this, the IER model is extended with operational refinements that preserve its zero-footprint principle and recursive geometry while increasing logistical flexibility. These include: (i) the incorporation of heterogeneous block sizes, (ii) the use of combined pulling and controlled pushing during final positioning, and (iii) progressive reduction of lane width at higher elevations.

Uniform block size is a common simplification in computational models of pyramid construction, enabling tractable estimates of transport time, workforce, and flow organization. However, archaeological evidence indicates that Old Kingdom block sizes were heterogeneous, varying spatially and with elevation, while internal composition remains only partly constrained. A single representative block mass should therefore be understood as a modeling abstraction, not a literal description of construction practice.

To assess its logistical effect, first-order scaling is considered. Required traction force increases approximately linearly with mass, so smaller blocks require smaller crews or lower instantaneous loads per worker. This benefit is offset by more transport cycles to deliver the same total volume.

In the baseline IER model, a ~2,268 kg block hauled on a 7.5° ramp with $\mu = 0.20$ requires ~24 pullers; under the same assumptions, a ~1,134 kg block requires ~12. Replacing one block with two smaller units preserves total mass and mechanical work but doubles transport cycles. Conversely, a ~4,536 kg load reduces cycles but increases team length and headway, producing diminishing returns. Thus, the ~24-puller estimate for a 2.27 t block is a mechanical lower bound. Ringelmann-type coordination losses [30] may reduce individual efficiency, while broader megalithic-transport constraints [31] highlight the importance of crew organization (two-abreast formation) and maneuverability (haul segments <~200 m).

On terraces, precise stone placement implies pushing during short-range positioning and final seating. Blocks had to be aligned and fitted against previously placed masonry with high precision, requiring localized force application not achievable through long-distance pulling alone.

At higher elevations, where ramp segments shorten and spatial constraints increase, hauling teams may have used mixed pulling–pushing configurations. A primary group at the front of the sledge could be complemented by a secondary group applying controlled rear force.

This does not alter the governing mechanics of transport, but redistributes force along the load, improving stability and maneuverability in confined sections and near turning points. Shorter upper-level transport distances further support this arrangement, as reduced fatigue and higher control demands favor compact, coordinated teams.

A further operational refinement is the progressive reduction of haul corridor width at higher elevations. In the baseline IER configuration, the active lane is defined by temporarily omitting 3×6 perimeter blocks. As the pyramid rises, working space, typical block size, and logistical demand per course decrease, making the full lower-stage corridor width unnecessary.

An upper-stage variant therefore reduces the active corridor to a 2×4 block omission above a defined elevation threshold. The same proportional scaling applies to corner maneuvering areas, with turning platforms reduced to a compact 3×3 geometry compatible with smaller loads and crews. This preserves the IER's recursive logic and zero-footprint principle while reducing temporary void volume, backfilling requirements, and spatial interference at height.

Within the model, this refinement is treated as a scaling adaptation rather than a change in construction principle. Its primary effect is not a reduction in traction force, but improved spatial efficiency, potentially delaying geometric saturation and enhancing maneuverability in the final construction stages.

The refinements introduced in Methods extend the baseline IER by incorporating operational adaptations that preserve the zero-footprint principle while increasing logistical flexibility. The following paragraphs present the Khafre-specific implications of these refinements under the same baseline IER assumptions used for G1, while retaining G2-specific geometry and boundary conditions. Quantitative estimates are reported where available; otherwise, results are framed as feasibility assessments consistent with Fourth-Dynasty constraints.

To assess block-size heterogeneity, we compare a standard 2,267.96 kg block with two 1,133.98 kg blocks transported sequentially, under common IER conditions for G1/G2 (θr ≈ 7.5°, μ = 0.20, v = 0.15 m/s, 2-abreast teams, 300 N/puller). Halving mass reduces the crew from 24 to 12 pullers and team length from 17.0 to 8.5 m, but sledge length and dynamic buffer remain fixed. Thus, total safety distance falls only from 35.0 to 26.5 m (~25%), and minimum headway from 3.89 to 2.94 min. Because the number of cycles doubles, total transport time for the same mass increases from 3.89 to 5.88 min (≈+51%), or up to 2.00× where final placement dominates.

Conversely, doubling the transported mass to ~4,536 kg load increases team length and headway (~34 m; ~5.78 min) but halves the number of cycles, giving a first-order transport-time factor of ~0.74× relative to the baseline. This apparent gain should be treated as an upper-bound estimate: larger blocks would likely increase corner-turning and alignment delays from the baseline ~3–4 min to perhaps ~5–6 min due to greater inertia, longer teams, and reduced maneuverability. However, because this remains comparable to the ~5.78 min safety headway, turning may be absorbed within the existing spacing constraint rather than becoming a separate dominant bottleneck. Overall, the system responds asymmetrically to block size: smaller blocks reduce instantaneous crew demand but penalize throughput, whereas larger blocks may improve throughput in principle but become more sensitive to maneuverability and geometric constraints. Table S4.1 summarizes the safety-distance budget and transport-time factors.

Table S4.1. Safety-distance budget and first-order relative transport time for double-size, standard, and half-size loads under IER ramp conditions ($\theta_r \approx 7.5°$, μ = 0.20, v = 0.15 m/s, two-abreast formation, 300 N per puller). The fixed 15 m dynamic buffer [14] prevents the reduction in team length from translating proportionally into a shorter headway. The lower bound of 1.51× assumes safety-distance-limited headway. With a larger transported load, the first-order transport time is theoretically 26% lower because the number of cycles is reduced.

	4,536 kg load	**2,268 kg block (base)**	**1,134 kg block**
Pullers	48	24	12
Team length	34 m (24 rows)	17.0 m (12 rows)	8.5 m (6 rows)
Sledge length	3.0 m	3.0 m	3.0 m
Dynamic buffer	15.0 m	15.0 m	15.0 m
Total safety distance	52.0 m	35.0 m	26.5 m
Minimum headway	5.78 min	3.89 min	2.94 min
Cycles per unit volume	0.5×	1×	2×
Relative transport time	0.74×	1.00×	1.51×

These results indicate a trade-off between block mass, crew size, maneuverability, and cycle number, suggesting that throughput would not scale linearly with block size. While total mechanical work remains proportional to transported mass, smaller blocks incur cycle-related penalties and larger blocks reduce maneuverability. Accordingly, transport organization is expected to favor minimizing the number of cycles rather than reducing mass per cycle, within the limits imposed by crew size and geometric constraints.

Under the adopted operational assumptions, moderate Ringelmann-type coordination losses only slightly increase nominal hauling requirements relative to the ideal mechanical estimate. For the baseline ~2,268 kg block transported on a 7.5° ramp with $\mu = 0.20$, the theoretical requirement of ~24 pullers is treated as a lower bound. Applying an efficiency factor of ~0.85 yields an operational estimate of ~28 pullers. This correction reflects the two-abreast team layout, pace regulators or supervisors at departure points and corner platforms, and short haul segments (<~200 m), all likely reducing the larger losses typical of bigger or less structured groups. Importantly, this adjustment does not modify the previously derived minimum headway of ~4 min for the Khufu IER baseline configuration (main-text Table 2 [14]), because team length remains compatible with safety-distance and corner-clearance assumptions. Overall, practical workforce requirements were probably somewhat higher than the idealized force-balance estimate, without affecting model feasibility.

A further upper-stage refinement considers reducing the active edge corridor from a three-block omission (3.81 m) to a two-block omission (2.54 m) above a defined elevation. To first order, this does not alter haul forces or total transport work, since slope and friction remain unchanged. Its effect is mainly geometric and operational: reducing temporary void volume, lowering backfilling demand, and increasing effective terrace space where base width becomes restrictive.

The expected benefit is not reduced per-block traction time, but mitigation of geometric saturation in the final phases. As upper-stage ramp segments shorten and block counts per course decrease, return traffic need not maintain a continuously open descending lane. Instead, descending teams may wait at corner platforms as controlled holding zones while ascending traffic passes. Corridor narrowing is therefore a space-optimization strategy, not a change in core IER mechanics.

The transition elevation is not prescribed a priori, but treated as an optimization parameter governed by geometry, traffic organization, maneuverability, and backfilling demand. If implemented, the threshold would likely be determined pragmatically, when the standard corridor became inefficient. Formal optimization is left for future simulation work.

In practical terms, this refinement yields second-order gains in maneuverability and spatial efficiency while leaving baseline feasibility unchanged. Its value lies in reducing local interference and preserving workable upper-stage geometry under diminishing base dimensions. It is especially relevant for Khafre (G2), where the steeper face restricts working space, but remains compatible with Khufu (G1) as a general IER adaptation. Although it does not directly increase throughput, it mitigates late-stage geometric bottlenecks that could degrade efficiency. The incorporation of combined pulling –pushing in final positioning does not modify the computational structure of the IER model, as it does not affect transport distances, headway, or system-level throughput. Its significance lies in improving the operational plausibility of block placement under constrained geometry.

Although feasibility has been explored computationally, full assessment requires dedicated physical experimentation. Final positioning involves short-range, high-precision movements under constrained conditions not fully captured by the transport model. Accordingly, placement times are excluded from the global schedule, and future experiments are needed to quantify their impact.

S5. Top-down backfilling and decommissioning strategies

Top-down closure of the IER channel is a distinct end-stage operation, not equivalent to standard block placement during ascent. Although minor in volume, final positioning follows different kinematics: backfilling blocks are hauled along the active ramp to near their final location, then maneuvered over short distances under confined conditions beside the open drop. This phase depends less on sustained traction than on controlled pushing, stabilization, and precise alignment. Experimental work by Denys Stocks [21] supports pushing and local manipulation for controlling heavy loads over short distances.

Because the open channel may span up to five courses (maximum ≈3.55 m), upper-row closure requires an auxiliary arrangement to bridge the height difference to the placement level. Two decommissioning variants are considered: (i) a short temporary ramp branching from the main IER lane, and (ii) a compact wedge-shaped embankment supported between the pyramid body and the open edge. In both cases, the final gradient is kept below ~20%, following the conservative short-distance limit associated with Hatnub quarry [34]. For a baseline IER slope of 7.5°, the auxiliary segment adds at most ~4°; in the embankment variant, the outer flank may reach ~60° while the inner side is supported against the masonry. These configurations are not presented as archaeologically demonstrated, but as mechanically plausible refinements.

This phase should be parameterized separately from standard placement. The original IER formulation for Khufu (G1) estimated transport time up to delivery from path length and dynamics, but did not resolve final seating during terrace positioning or channel closure. Its schedule impact is expected to remain limited because the affected volume is small, the active channel remained several meters wide per course, and controlled placement of standard-sized blocks could restore the pyramid geometry without necessarily producing visually distinct micro-masonry, irregular infill, or clear macroscopic ramp signatures on the upper casing.

In the temporary-ramp variant, closure proceeds top-down through localized dismantling, block placement, and progressive ramp construction. Temporary infill is partly removed to restore a flat working surface at the completed course; blocks are placed from the inner side outward in contiguous groups for stability; and, after the first row, a short ramp from the main IER lane overcomes the one-course vertical offset (≈0.71 m). From the third step onward, upper rows are completed while lower sections begin filling, so the ramp advances downward recursively while maintaining delivery access. To keep the added slope to ~4° and the total below ~20%, ramp length increases with elevation difference; in the most demanding case, ~five courses (~3.55 m), it reaches ~18 m. A few corner blocks may remain difficult to insert, but they represent a negligible fraction of total volume and require experimental assessment rather than system-level redesign. Continued downward, the sequence closes the channel with the blocks reserved for its formation, leaving no substantial external trace.

In the wedge-shaped embankment variant (Fig. S5.1), the area is likewise re-levelled, but a compact sloped embankment increases maneuvering space in the upper rows. For a closure height of ~five courses (≈3.55 m) and a base width of 3.81 m, the pyramid face (53.13°) provides ~1.15 m of clearance, whereas a 60° embankment reduces the horizontal projection to ~2.05 m and increases clearance to ~1.76 m (+0.61 m). Operationally, lower rows are placed first from the inner side outward, leaving the outer casing position temporarily unset; as each row is completed, the auxiliary ramp and embankment are extended, with the outer flank serving as access surface and the inner side supported by placed masonry. The system grows to ~18 m for the fifth row, remains below ~20% gradient, and is then dismantled from top to bottom while remaining outer blocks are set. This repeatable build-and-remove cycle reduces critical upper-level placement constraints compared with the narrow-ramp variant, although it adds local complexity.

Overall, these simulations do not provide precise time estimates, but indicate that channel closure is mechanically plausible, geometrically consistent, repeatable, and compatible with restricted space. In both variants, final positioning relies on small teams performing short-range controlled movements for alignment and stabilization rather than sustained hauling, without requiring additional large-scale structures beyond those already included in the IER framework.

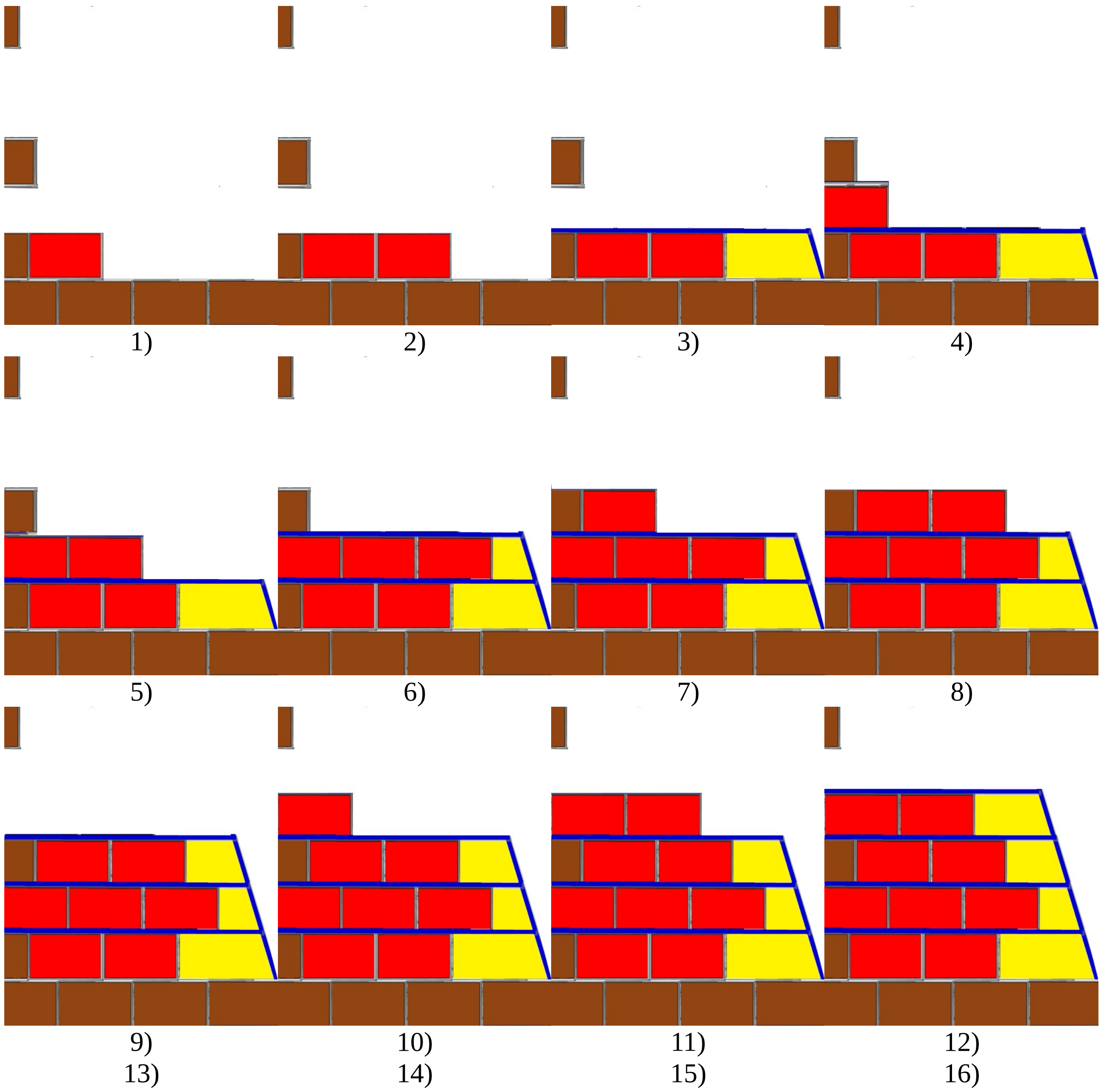

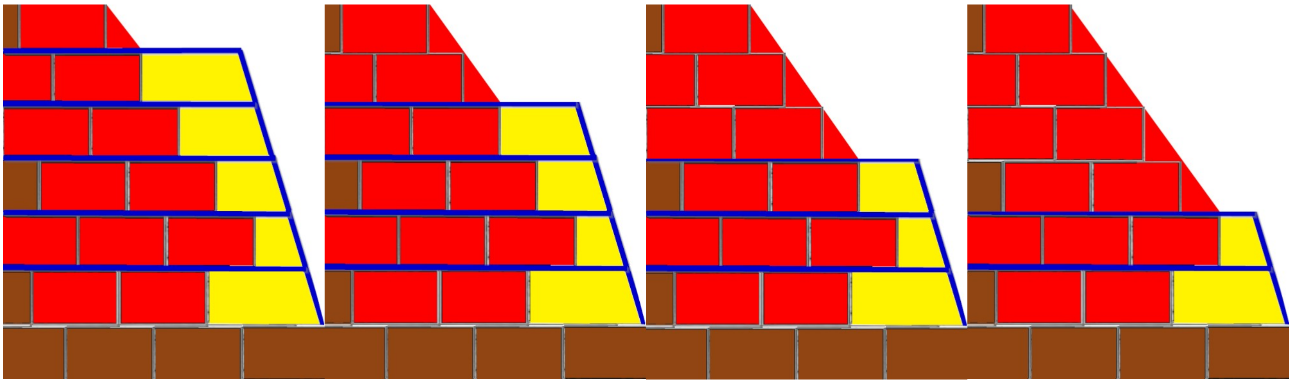

17) 18) 19) 20)

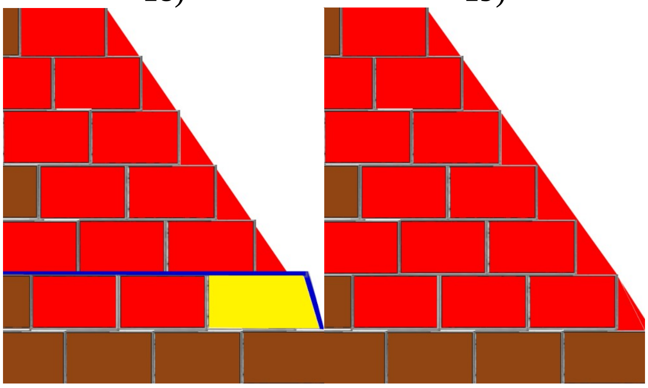

21) 22)

Fig. S5.1. Step-by-step implementation of the wedge-shaped embankment strategy for top-down closure of the edge-integrated channel. The sequence represents a localized, repeatable operation applied to successive channel segments during the final decommissioning phase. The sequence is shown for a representative five-course closure (~3.55 m), but the procedure is scale-independent and can be applied to different channel heights. Red blocks represent placed masonry, the yellow areas represent the temporary embankment, and the blue outlines indicate the embankment limit at each course.

The corresponding time-lapse sequences are provided as Supplementary Videos 1–2.

S6. Semi-automatic extraction of course-height profiles

Course-height profiles were extracted from high-resolution frontal images of the Pyramid of Khafre using a semi-automatic line-detection workflow developed by the author. Visible masonry courses were manually traced using horizontal guide lines, after which the software identified line centroids and merged adjacent detections within a configurable pixel threshold. Vertical pixel spacing between detected courses was then converted into approximate real dimensions using the known visible height of the pyramid as a scaling reference. The method was not intended to provide absolute architectural metrology, but rather to identify relative variations in course thickness, discontinuities, and large-scale geometric patterns observable across the pyramid faces. The extracted profile is therefore used only to support a semi-qualitative classification of course-height regimes, not to establish absolute elevations or statistically independent measurements.

Fig. S6.1. Semi-automatic extraction of masonry-course profiles from a frontal image of the Pyramid of Khafre. Horizontal guide lines (blue) were manually aligned with visually identifiable masonry courses across the pyramid face and subsequently processed using a custom line-detection workflow developed by the author. The software identifies line centroids, merges adjacent detections within a configurable threshold, and converts vertical pixel spacing into approximate real course heights using the known visible height of the pyramid as a scaling reference. The method is intended to detect relative variations in course thickness, discontinuities, and large-scale geometric patterns rather than to provide absolute architectural metrology. Photo by Carlota O. on Unsplash, used under the Unsplash license (accessed January 31, 2026), blue lines created by the author.

The numerical values extracted through the semi-automatic workflow should not be interpreted as precise architectural measurements, since they are affected by perspective distortion, erosion, image resolution, and the approximate nature of the line-tracing process. Instead, the workflow is used to construct a semi-qualitative classification of course thicknesses, identifying relative regimes and transitions across the pyramid body. Based on the detected height ranges, courses are grouped into a reduced set of operational categories used in the geometric-logistic model (main-text Table 1). These categories represent simplified construction regimes rather than exact in-situ dimensions, allowing the model to capture large-scale organizational patterns while remaining robust against local measurement uncertainty.